mathematics

MDPI

Article

Decentralized Adaptive Event-Triggered Fault-Tolerant Cooperative Control of Multiple Unmanned Aerial Vehicles and Unmanned Ground Vehicles with Prescribed Performance under Denial-of-Service Attacks

Shangkun Liu and Jie Huang *

College of Electrical Engineering and Automation, Fuzhou University, Fuzhou 350108, China; shangkunliu@fzu.edu.cn

* Correspondence: jie.huang@fzu.edu.cn

Abstract: This paper proposes a decentralized adaptive event-triggered fault-tolerant cooperative control (ET-FTCC) scheme for multiple unmanned aerial vehicles (UAVs) and unmanned ground vehicles (UGVs) with actuator faults and external disturbances under denial-of-service (DoS) attacks. The multiple UAVs and UGVs have a larger search radius, which is important in both the civilian and military domains. The different dynamics between UAVs and UGVs result in unbalanced interactions in the communication topologies, which increases the complexity of cooperative control. DoS attacks are conducted in both sensor and control channels. The dynamic models of UAVs and UGVs are introduced firstly, and the unified heterogeneous multiagent system model with actuator faults is established. The composite observer is designed to obtain the information of state and lumped disturbance, which is used to design the controller. In order to save the limited communication network resources, the event-triggered mechanism is introduced. The transformed error is presented by using the prescribed performance function (PPF). Then, the sliding-mode manifold is presented by combining the event-triggered control scheme to achieve the tracking purpose with actuator faults, external disturbances, and DoS attacks. Based on the Lyapunov function approach, the tracking errors are bounded within the prescribed boundary. Finally, the effectiveness of the proposed method is verified by qualitative analysis and quantitative analysis of the simulation results. This study can enhance the security and reliability of heterogeneous multiagent systems, providing technical support for the safe operation of unmanned systems. This paper mainly solves the FTCC problem of second-order nonlinear heterogeneous multiagent systems, and further research is needed for the FTCC problem of higher-order nonlinear heterogeneous multi-agent systems. In addition, the system may encounter multiple cyber attacks. As one of the future research works, we can extend the results of this paper to high-order nonlinear systems under multiple cyber attacks, which contain DoS attacks and deception attacks, and achieve fault-tolerant cooperative control of heterogeneous multiagent systems.

Keywords: fault-tolerant cooperative control; event-triggered mechanism; prescribed performance function; DoS attacks; heterogeneous multiagent systems

MSC: 93A16; 93C40

Citation: Liu, S.; Huang, J. Decentralized Adaptive Event-Triggered Fault-Tolerant Cooperative Control of Multiple Unmanned Aerial Vehicles and Unmanned Ground Vehicles with Prescribed Performance under Denial-of-Service Attacks. *Mathematics* **2024**, *12*, 2701. https://doi.org/10.3390/math12172701

Academic Editor: Mudassir M. Rashid

Received: 14 August 2024
Revised: 26 August 2024
Accepted: 29 August 2024
Published: 29 August 2024

1. Introduction

Heterogeneous multiagent systems (HMASs) are widely employed in many fields, such as area searching, spacecraft formation flying, and so on [1–3]. An HMAS consists of different types of agents that offer more advantages than the homogeneous MASs. For example, multiple UAVs and UGVs have a larger search radius, which is important in both the civilian and military domains. However, due to the heterogeneous characteristics

such as structure, and state dimensions between UAVs and UGVs, the execution of air ground formation tasks is hindered. Due to the heterogeneous characteristics of UAVs and UGVs, as well as the influence of parameter uncertainties, air–ground heterogeneous tracking control faces several challenges: UAVs and UGVs differ notably in structure, state dimensions, and model parameters; faults in the physical layer and DoS attacks in the cyber layer of multiple UAVs and UGVs may affect tracking performance. Recently, various cooperative control issues have been investigated for MASs to achieve consensus, formation, or containment control [4–6]. But, the existing cooperative control strategies illustrated may not be directly scalable to the cooperative control of HMASs, since there are unexpected actuator faults and DoS attacks.

In practical applications, the actuator in the physical layer may encounter faults. Because the agent is connected through the communication topology, faults will spread through the network, and may result in critical destruction of the system. To ensure the systems' safe operation, fault-tolerant control (FTC) is an efficient method, and has drawn much attention in safety-critical systems [7–9]. In [10], the fault-tolerant tracking control based on distributed observer for MASs is investigated under directed topology. In [11], the FTC protocol utilizing local state information of neighbor agents is presented for MASs subjected to actuator faults. In [12], the FTC scheme by using distributed observer and auxiliary controller gain is investigated for MASs subjected to actuator faults. In [13], the distributed FTC strategy is presented for nonlinear MASs with external disturbances under switched topologies. Nevertheless, in addition to faults in physical layer, attacks in cyber layer can also block the transmission of information, which can be very destructive. In [14], the distributed FTC scheme is investigated by utilizing fuzzy logic systems method and switching mechanism for MASs with node fault and DoS attacks. In [15], the distributed FTC protocol based on resilient observer for HMASs is illustrated under DoS attacks. In [16], the distributed output-feedback control strategy is presented for linear HMASs with sampling and random DoS attacks. In [17], the distributed consensus problem is studied for MASs subjected to DoS attacks under directed topology. In [18], the distributed formation control strategy is designed for MASs against DoS attacks. However, there are few results on FTCC of HMASs with actuator faults subjected to DoS attacks.

Transient performance is another important problem for tracking control of MASs; it is significant to take transient and steady-state performance into account in the post-fault phase. In [19], the adaptive FTC scheme which can ensure that the consensus errors satisfy the prescribed performance requirements is investigated for nonlinear MASs. In [20], the prescribed performance control strategy is presented for a vehicular platoon by utilizing a Gaussian error function and finite-time PPF. In [21], the finite-time consensus issue is illustrated for MASs within prescribed performance. In [22], the tracking control issue is presented for underwater vehicle with model uncertainties by using PPF and disturbance observer. In [23], the formation-containment control scheme is presented for HMASs with prescribed performance. Also considering the limited communication resource, the event-triggered mechanism is proposed to obtain better performance with limited communication resources. In [24], the distributed ET containment control scheme by using a disturbance observer, which does not require the continuous sharing of state information, is studied for linear MASs with DoS attack and external disturbances. In [25], the distributed ET consensus problem is presented for linear MASs under DoS jamming attacks. In [26], the distributed ET formation control scheme is investigated for nonlinear MASs against DoS attacks. In [27], the ET consensus issue is studied for linear MASs with frequency cyber attacks. Although several FTC strategies are investigated for MASs under DoS attacks, the adaptive ET-FTCC strategy for HMASs with actuator faults and prescribed performance against DoS attacks is a challenging problem.

Motivated by the above-mentioned analyses, this paper investigates the ET-FTCC scheme for HMASs with actuator faults subjected to DoS attacks. The observer is designed to obtain the unmeasurable states. The PPF is utilized to convert the tracking error. Utilizing the transformed error, the ET-FTCC with prescribed performance can be achieved.

In comparison with other relevant works, the main contributions are concluded as follows:

1. In order to save the limited communication network resources, the novel ET mechanism is illustrated, in comparison with some existing results [28,29], in which only the ET mechanism in the control channel is considered. The event-triggered mechanism is also presented by using the triggered state directly, which may cause chattering of the controller once actuator faults or DoS attacks occur. In this work, the ET mechanism in the sensor and controller channel are both considered. The presented ET mechanism can balance the limited communication network resources and information utilization. Furthermore, the Zeno behavior is excluded.
2. The composite observer is presented, in which the state is estimated and the lumped disturbances are reconstructed utilizing the estimated state and the sensor channel triggered outputs without using the disturbance upper bound. In this way, the unknown variables are estimated with less information. In contrast to some existing results [30,31], in which the upper bound information of disturbances should be known when designing the disturbance observer, the results of this work provide another method to estimate the disturbances.
3. An observer-based ET-FTCC scheme, including FTC compensation, disturbances degradation, and DoS prevention components, is studied. To obtain good system performance, a modified PPF is presented to convert the tracking errors, thereby relaxing the requirement for the exact initial conditions. In contrast to the work in [32], in which the control input is blocked when the DoS attack is active, the data at the instant when the attacker is switched between asleep and active in this work is triggered and utilized as a compensation component.

The remainder of this paper is presented as follows. Some preliminaries and problem formulation are introduced in Sections 2 and 3. Section 4 gives the main theoretical results. The simulation studies are provided in Section 5. Section 6 concludes the paper.

2. Preliminaries

2.1. Graph Theory

A graph is given to describe interaction topology of agents. The undirected graph $\mathcal{G} = (\mathcal{V}, \mathcal{E})$ consists of a node set $\mathcal{V} = \{1, 2, \ldots, N\}$ and an edge set $\mathcal{E} \subseteq \mathcal{V} \times \mathcal{V}$. Let $\mathcal{A} = [a_{ij}] \in R^{N\times N}$ be adjacency matrix of $\mathcal{G}$, where $a_{ij} = 1$ if $(j, i) \in \mathcal{E}$ and $a_{ij} = 0$ otherwise. Let $\mathcal{D} = \text{diag}\{d_1, d_2, \ldots, d_N\}$ be degree matrix with $d_i = \sum_{j=1}^{N} a_{ij}$. The Laplacian matrix is defined as $\mathcal{L} = [l_{ij}] = \mathcal{D} - \mathcal{A} \in R^{N\times N}$.

Assumption 1. *The topology $\mathcal{G}$ is connected.*

Lemma 1 ([33])**.** *If Assumption 1 is satisfied and $\mathcal{U} \in R^N$ is a nonzero non-negative vector, then $\mathcal{L}$ and $\mathcal{L} + \text{diag}(\mathcal{U})$ are both symmetric positive definite matrices.*

2.2. Actuator Fault Model

The actuator fault model is presented as

$$u_{ih}^F(t) = \rho_{ih} u_{ih}(t) + u_{ihb}(t), \tag{1}$$

where ρ_{ih} denotes the unknown effectiveness factor, $u_{ihb}(t)$ denotes the bias, $u_{ih}(t)$ and $u_{ih}^F(t)$ denote the desired and actual control input signal.

From (1), one has

$$u_i^F(t) = \rho_i u_i(t) + u_{ib}(t), \tag{2}$$

with $\rho_i = \text{diag}\{\rho_{i1}, \rho_{i2}, \ldots, \rho_{in}\}$, $u_{ib}(t) = [u_{ib1}(t), u_{ib2}(t), \ldots, u_{ibn}(t)]^T$.

Assumption 2. *There exist a lower bound* $\underline{\rho}_i$ *and upper bound* $\bar{\rho}_i$ *satisfying* $0 < \underline{\rho}_i \leq \rho_i \leq \bar{\rho}_i \leq 1$. $\|\dot{\rho}_i\| \leq \rho_{ic}$ *with* ρ_{ic} *being a positive constant.*

2.3. DoS Attack Model

DoS attacks can interfere with the communication channel and damage the communication equipment, causing data transmission to be interrupted. It can attack the single communication channel or attack measurement, communication, and control channels all at once. The DoS attack has great destructive power, but it needs to stop to recover energy, due to energy limitations. The attack's purpose is to obliterate the transmitted data before reaching the destination, which is expressed as

$$\mathcal{S}_{DoS} = \begin{cases} 0, \ t \in \Xi_{n,1} := [p_{dn}, p_{dn} + l_{dn}), \\ 1, \ t \in \Xi_{n,2} := [p_{dn} + l_{dn}, p_{dn+1}), \end{cases} \tag{3}$$

where p_{dn} and l_{dn} represent the instant and the length of the n-th attack, respectively. $\Xi_{n,1}$ and $\Xi_{n,2}$ represent the sleeping period and active period of the DoS attack, respectively.

Assumption 3. *Let* $n_a(\tau_d, t)$ *be the number of attacks on* $[\tau_d, t)$*; there exist* $\xi_d \geq 0$ *and* $\tau_S > 0$ *satisfying*

$$n_a(\tau_d, t) \leq \xi_d + \frac{t - \tau_d}{\tau_S}.$$

Assumption 4. *Let* $|\Xi(\tau, t)|$ *be the length of* $\Xi(\tau_d, t)$*; there exist* $o_d \geq 0$ *and* $T > 1$ *satisfying*

$$|\Xi(\tau, t)| \leq o_d + \frac{t - \tau_d}{T}.$$

3. Problem Formulation

In this section, M_1 quadrotor UAVs and M_2 two-wheeled mobile robot UGVs are considered. For convenience, let $\Pi_1 = \{1, 2, \ldots, M_1\}$, $\Pi_2 = \{M_1 + 1, M_1 + 2, \ldots, M_1 + M_2\}$, and $\Pi = \Pi_1 \bigcup \Pi_2$.

3.1. UAV Dynamics

The structure of the quadrotor UAV is shown in Figure 1. In order to describe the dynamic characteristic of the quadrotor UAV, the inertia frame and the body-fixed frame are employed. The axes of the inertia frame are denoted as (x_e, y_e, z_e), and the axes of the body-fixed frame are denoted as (x_b, y_b, z_b). The translational dynamics of the i-th ($i \in \Pi_1$) UAV are described as [34]

$$\begin{cases} m_{ai}\ddot{p}_{aix} = (\cos\phi_{ai}\sin\theta_{ai}\cos\psi_{ai} + \sin\phi_{ai}\sin\psi_{ai})u_{pi} - d_{ix}\dot{p}_{aix}, \\ m_{ai}\ddot{p}_{aiy} = (\cos\phi_{ai}\sin\theta_{ai}\sin\psi_{ai} + \sin\phi_{ai}\cos\psi_{ai})u_{pi} - d_{iy}\dot{p}_{aiy}, \\ m_{ai}\ddot{p}_{aiz} = (\cos\theta_{ai}\cos\phi_{ai})u_{pi} - m_{ai}g - d_{iz}\dot{p}_{aiz}, \end{cases} \tag{4}$$

$$\begin{cases} J_{ax}\ddot{\phi}_{ai} = \dot{\theta}_{ai}\dot{\psi}_{ai}(J_{ay} - J_{az}) - J_{ar}\dot{\theta}_{ai}\bar{d}_{ai} + \tau_{\phi i} - d_{i\phi}\dot{\phi}_{ai}, \\ J_{ay}\ddot{\theta}_{ai} = \dot{\phi}_{ai}\dot{\psi}_{ai}(J_{az} - J_{ax}) - J_{ar}\dot{\phi}_{ai}\bar{d}_{ai} + \tau_{\theta i} - d_{i\theta}\dot{\theta}_{ai}, \\ J_{az}\ddot{\psi}_{ai} = \dot{\phi}_{ai}\dot{\theta}_{ai}(J_{ax} - J_{ay}) + \tau_{\psi i} - d_{i\psi}\dot{\psi}_{ai}, \end{cases} \tag{5}$$

where $[p_{aix}, p_{aiy}, p_{aiz}]^T$ and $[\phi_{ai}, \theta_{ai}, \psi_{ai}]^T$ denote the position and attitude states, d_{ix}, d_{iy}, and d_{iz} denote the aerodynamic damping coefficients, m_{ai}, u_{pi}, and g denote the mass, control thrust, and gravitational acceleration, $\tau_{\phi i}$, $\tau_{\theta i}$, and $\tau_{\psi i}$ denote the three control torques, J_{ax}, J_{ay}, and J_{az} denote the moments of the inertia, J_{ar} denotes the moment of rotor's inertia, and $\bar{d}_{ai}$ is the overall residual rotor angle.

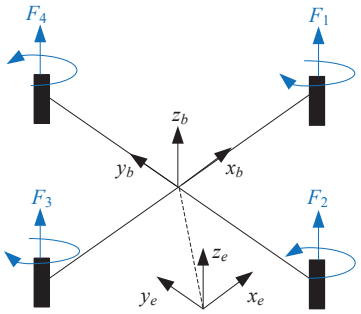

Figure 1. The structure of the quadrotor UAV.

Consider a new control signal u_{ai}; (4) can be rewritten as

$$\ddot{p}_{ai} = u_{ai} + f_{ai}, \tag{6}$$

where $f_{ai} = [-d_{ix}\dot{p}_{aix}/m_{ai}, -d_{iy}\dot{p}_{aiy}/m_{ai}, -d_{iz}\dot{p}_{aiz}/m_{ai} - g]^T$, $p_{ai} = [p_{aix}, p_{aiy}, p_{aiz}]^T$, $u_{ai} = [u_{aix}, u_{aiy}, u_{aiz}]^T$ with $u_{aix} = (\cos\phi_{ai}\sin\theta_{ai}\cos\psi_{ai} + \sin\phi_{ai}\sin\psi_{ai})u_{pi}/m_{ai}$, $u_{aiy} = (\cos\phi_{ai}\sin\theta_{ai}\sin\psi_{ai} - \sin\phi_{ai}\cos\psi_{ai})u_{pi}/m_{ai}$, $u_{aiz} = (\cos\phi_{ai}\cos\theta_{ai})u_{pi}/m_{ai} - g$.

Remark 1. *The six-degree-of-freedom quadrotor dynamic systems can be controlled by utilizing attitude subsystems and trajectory subsystems control framework. The trajectory subsystems, which are capable of guiding the quadrotor UAV to an expected position, are more significant in the UAV tracking control design than the attitude subsystems [35]. Therefore, the adaptive event-triggered fault-tolerant cooperative control scheme studied in this paper considers the trajectory systems.*

3.2. UGV Dynamics

The two-wheeled mobile robot UGV is driven by two wheels at the rear, with a supporting universal wheel at the front to maintain stability. The structure of the UGV is shown in Figure 2. The dynamic model of the i-th ($i \in \Pi_2$) two-wheeled mobile robot UGV is described as [36]

$$\begin{cases} \dot{x}_{gi} &= v_{gi}\cos\theta_{gi}, \\ \dot{y}_{gi} &= v_{gi}\sin\theta_{gi}, \\ \dot{\theta}_{gi} &= \omega_{gi}, \end{cases} \tag{7}$$

where $x_i = [x_{gi}, y_{gi}]^T$ denotes the position states, θ_{gi} denotes the orientation, v_{gi} and ω_{gi} are the linear and angular velocity, respectively, $\dot{v}_{gi} = F_{gi}/M_{gi}$, $\dot{\omega}_{gi} = \tau_{gi}/J_{gi}$, M_{gi} and J_{gi} are the mass and moment of the inertia, and F_{gi} and τ_{gi} are the force and torque.

Due to the non-holonomic constraint, a hand position approach is utilized. The front point (p_{gix}, p_{giy}) of the UGVs is defined as the hand point. The coordinate transformation is given as $p_{gix} = x_{gi} + L_{gi}\cos\theta_{gi}$ and $p_{giy} = y_{gi} + L_{gi}\sin\theta_{gi}$, where L_{gi} is the distance between the position (x_{gi}, y_{gi}) and the new defined hand point (p_{gix}, p_{giy}). Then, the system (7) is rewritten

$$\ddot{p}_{gi} = u_{gi} + f_{gi}, \tag{8}$$

where

$$u_{gi} = \begin{bmatrix} \cos\theta_{gi} & -L_{gi}\sin\theta_{gi} \\ \sin\theta_{gi} & L_{gi}\cos\theta_{gi} \end{bmatrix} \begin{bmatrix} \dot{v}_{gi} \\ \dot{\omega}_{gi} \end{bmatrix},$$
$$f_{gi} = \begin{bmatrix} -v_i\omega_{gi}\sin\theta_{gi} - L_{gi}\omega_{gi}^2\cos\theta_{gi} \\ v_i\omega_{gi}\cos\theta_{gi} - L_{gi}\omega_{gi}^2\sin\theta_{gi} \end{bmatrix}.$$

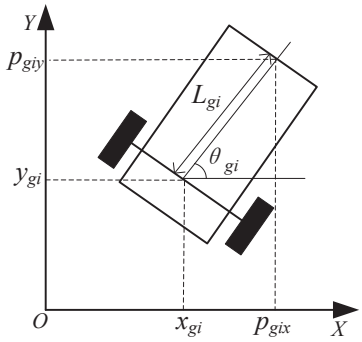

Figure 2. The structure of the UGV.

3.3. Model Transformation

In comparison with MASs, the difficulty of cooperative control of HMASs is that the dynamic characteristics and even the dimensions differ between the agents. To solve this control problem, the unified control model with actuator faults model (2) and external disturbances d_i is written as

$$\begin{cases} \dot{x}_{i1} = x_{i2}, \\ \dot{x}_{i2} = \rho_i u_i + u_{ib} + d_i + f_i, \end{cases} \tag{9}$$

where $x_{i1} = [p_{aix}, p_{aiy}, p_{aiz}]^T$ denotes the position of the i-th UAV, $\rho_i = \text{diag}\{\rho_{aix}, \rho_{aiy}, \rho_{aiz}\}$ denotes the effectiveness factor, $u_i = [u_{aix}, u_{aiy}, u_{aiz}]^T$ denotes the virtual control input signal, $f_i = f_{ai}$ denotes the nonlinear term, $u_{ib} = [u_{aibx}, u_{aiby}, u_{aibz}]^T$ denotes the bias, $d_i = [d_{aix}, d_{aiy}, d_{aiz}]^T$ denotes the external disturbance ($i \in \Pi_1$), $x_{i1} = [p_{gix}, p_{giy}, 0]^T$ denotes the position of the i-th UGV, $\rho_i = \text{diag}\{\rho_{gix}, \rho_{giy}, 0\}$ denotes the effectiveness factor, $u_i = [u_{gix}, u_{giy}, 0]^T$ denotes the virtual control input signals, $f_i = f_{gi}$ denotes the nonlinear term, $u_{ib} = [u_{gibx}, u_{giby}, 0]^T$ denotes the bias, and $d_i = [d_{gix}, d_{giy}, 0]^T$ denotes the external disturbance, $i \in \Pi_2$.

Hence, (9) can be rewritten as

$$\dot{x}_i = A_i x_i(t) + B_i \rho_i u_i(t) + R_i(t), \tag{10}$$

where $A_i = \begin{bmatrix} 0 & 1 \\ 0 & 0 \end{bmatrix}$, $B_i = [0, 1]^T$, $R_i(t) = B_i d_i + B_i u_{ib} + B_i f_i$.

Remark 2. *Since the dynamics of UAVs and UGVs are three dimensional and two dimensional, respectively, it is hard to design collaborative control scheme straightforwardly. Hence, the dimension of the UGV is upgraded, i.e., the position, velocity, and control input on Z-axis are zero. In addition, the unified control model (9) is transformed from the actual physical models of quadrotor UAVs and two-wheeled mobile robot UGVs; therefore, the complexity of UAVs and UGVs can be reflected. Consequently, the unified control model (9) accommodates both UAVs and UGVs.*

3.4. Control Objective

The control objective is to present ET-FTCC scheme for HMASs (9) subjected to actuator faults and disturbances against DoS attacks, such that the tracking errors can be restrained to the prescribed bounds.

4. Main Results

In this section, the ET-FTCC scheme is designed for HMASs subjected actuator faults and disturbances against DoS attacks. Figure 3 shows the diagram.

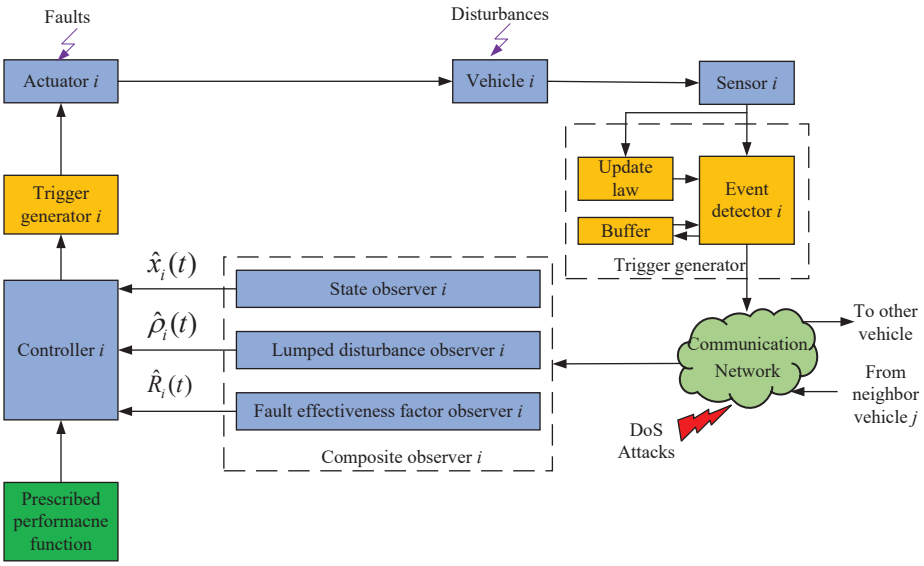

Figure 3. The diagram of ET-FTCC scheme.

4.1. Event-Triggered Mechanism Design

To save the limited communication resource, the ET mechanism in the sensor and controller channel are both considered. For the sensor channel, the ET time instants are designed as

$$t^i_{k+1}h = \inf\{qh > t^i_k h : \mathcal{F}_i(qh) > 0\}, \tag{11}$$

where $\mathcal{F}_i(qh) = e_{zi}(t^i_k h)^T \mathcal{Q}_i e_{zi}(t^i_k h) - \sigma \epsilon_i(t^i_k h + qh)^T \mathcal{Q}_i \epsilon_i(t^i_k h + qh)$, with $\sigma \in [0,1)$, $\mathcal{Q}_i > 0$, $q \in N$, $e_{zi}(t^i_k h) = y_i(t^i_k h) - y_i(t^i_k h + qh)$, $\epsilon_i(t^i_k h + qh) = \sum_{j \in N_i} a_{ij}[y_i(t^i_k h + qh) - y_j(t^j_k h + qh)]$.

The DoS attack can interfere with communication channel, which indicates that the k-th triggered data may not be delivered to the target when the DoS attack is active. Figure 4 shows an example of the ET mechanism and sequence of DoS attacks. In Figure 4, the n-th DoS attack period Ξ_n includes the sleeping period $\Xi_{n,1}$ and the active period $\Xi_{n,2}$. To ensure the performance, the reasonable assumption is made that the packets at the end of each attack period p_{dn} should be released regardless of whether it satisfies the condition (11) in the ET mechanism. The specific meaning of each kind of packet is shown in Figure 4. For example, at instant $10h$, the packet does not satisfy the condition (11), but it is necessary to improve the performance. Hence, the resilient ET mechanism is given as

$$t^i_{k,n+1}h \in \{t^i_s h \text{ satisfying } (11) | t^i_s h \in \Xi_{n,1}\} \cup \{p_{dn}\}, \tag{12}$$

where $t^i_{k,n+1}h$ denotes the instant when the data are transmitted to sensor. $k \in \{0, 1, \cdots, k(n)\}$ with $k(n) = \sup\{k \in N | t^i_{k,n+1}h < p_{dn} + l_{dn}\}$.

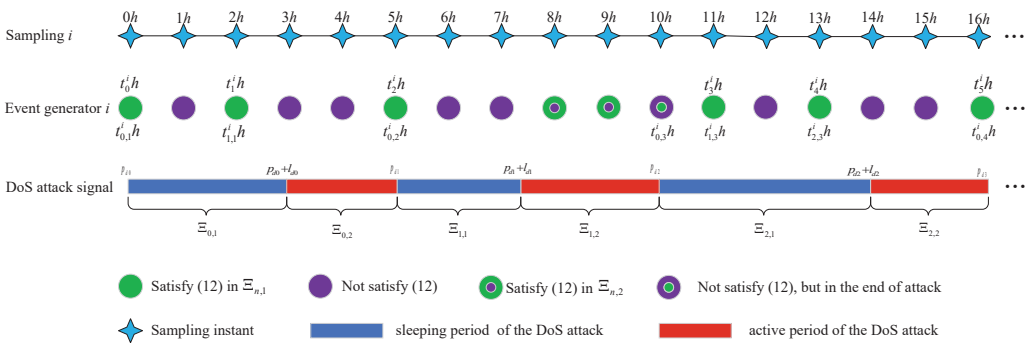

Figure 4. Example of the ET mechanism and sequence of DoS attacks.

Remark 3. *According to Equation (11), the next transferred data will be triggered if the condition is met. Since the DoS attacks can block the communication, the triggered data should not be within the active period of the DoS attacks. Hence, the resilient ET mechanism (12) is proposed.*

4.2. Observer Design

The state of the HMASs is treated as not fully measurable; the observer is presented for (10) at $t \in [t_k^i h, t_{k+1}^i h)$

$$\begin{cases} \dot{\hat{x}}_i(t) = A_i\hat{x}_i(t) + B_i\hat{\rho}_i u_i(t) + L_i(y_i(t_{k,n+1}^i h) - \hat{y}_i(t)) + \Delta_i(t), \\ \hat{y}_i(t) = C_i\hat{x}_i(t), \end{cases} \tag{13}$$

where $\hat{x}_i(t)$, $\hat{\rho}_i$, $\hat{\theta}_i$, and $\hat{y}_i(t)$ denote the estimations of $x_i(t)$, ρ_i, θ_i^*, and $y_i(t)$, respectively. L_i denotes observer gain. $\Delta_i(t)$ is an estimation error compensator, which is given as

$$\begin{aligned} \Delta_i(t) = \frac{P_i e_{xi}(t)}{\|e_{xi}(t)^T P_i\|^2} \Big(& \hat{\iota}_i \Big\| e_{xi}(t)^T P_i \Big\| \Psi_i(t) - \kappa_1 \|\Psi_i(t)\|^2 \\ & - \Big\| e_{xi}(t)^T P_i L_{ci} e_{xi}(t) \Big\| - \Big\| e_{xi}(t)^T P_i L_i e_{yi}(t) \Big\| + \eta_{ci} \Big), \end{aligned} \tag{14}$$

where $e_{xi}(t) = x_i(t) - \hat{x}_i(t)$, $e_{yi}(t) = y_i(t_{k,n+1}^i h) - y_i(t)$, $\eta_{ci} = (\bar{\rho}_i - \underline{\rho}_i)(\bar{\rho}_i - \underline{\rho}_i + \rho_{ic})$, P_i is a positive symmetry matrix, L_{ci} is a designed matrix, $\hat{\iota}_i$ is the estimations of ι_i, and κ_1 is a positive constant.

The adaptive law of $\hat{\rho}_i$ is designed as

$$\dot{\hat{\rho}}_i = \mathrm{Proj}_{[\underline{\rho}_i, \bar{\rho}_i]}\{\mathcal{P}\} = \begin{cases} 0, & \text{if } \hat{\rho}_i = \bar{\rho}_i \text{ and } \mathcal{P} \geq 0 \\ & \text{or } \hat{\rho}_i = \underline{\rho}_i \text{ and } \mathcal{P} \leq 0, \\ \mathcal{P}, & \text{otherwise,} \end{cases} \tag{15}$$

where $\mathcal{P} = -B_i u_i(t)^T P_i e_{xi}(t)$.

Hence, the error system is obtained as

$$\dot{e}_{xi}(t) = B_i\tilde{\rho}_i u_i(t) + (A_i - L_i C_i)e_{xi}(t) + R_i(t) - L_i e_{yi}(t) - \Delta_i(t) \tag{16}$$

where $\tilde{\rho}_i = \rho_i - \hat{\rho}_i$.

In this work, the lumped disturbance is assumed to meet $R_i(t) \leq \iota_i\|\Psi_i(t)\|$, with ι_i being an unknown constant. The auxiliary vector is given as

$$\Psi_i(t) = \int_0^t \kappa_2 e_{xi}(t)dt + e_{xi}(t) - \xi_i(t), \tag{17}$$

with κ_2 being a positive constant. $\xi_i(t)$ is an internal variable, which is given as

$$\begin{aligned} \dot{\xi}_i(t) = {} & B_i\tilde{\rho}_i u_i(t) + (A_i - L_i C_i)e_{xi}(t) + (\kappa_1 + \hat{\iota}_i)\Psi_i(t) \\ & + \kappa_2 e_{xi}(t) - L_i e_{yi}(t) - \Delta_i(t). \end{aligned} \tag{18}$$

The adaptive law $\hat{\iota}_i$ is designed as

$$\dot{\hat{\iota}}_i = \kappa_1(\|\Psi_i(t)\|^2 + \|e_{xi}^T(t)P_i\|\|\Psi_i(t)\|). \tag{19}$$

In addition, the lumped disturbances can be estimated as

$$\dot{\hat{R}}_i(t) = (\kappa_1 + \hat{\iota}_i)\Psi_i(t). \tag{20}$$

Theorem 1. *With the estimators (13) and (20), and the adaptive law (15), the estimation errors of the close-loop systems is guaranteed if the following condition holds:*

$$(P\Gamma + PL_c)^T + (P\Gamma + PL_c) < 0, \tag{21}$$

with $P = \mathrm{diag}\{P_1, P_2, \cdots, P_N\}$, $L_c = \mathrm{diag}\{L_{c1}, L_{c2}, \cdots, L_{cN}\}$, $\Gamma = [A_1 - L_1C_1, A_2 - L_2C_2, \cdots, A_N - L_NC_N]$.

Proof. Consider the Lyapunov function

$$V_1(t) = \sum_{i=1}^{N}(e_{xi}^T(t)P_ie_{xi}(t) + \Psi_i(t)\Psi_i(t) + \frac{\tilde{\iota}_i^T\tilde{\iota}_i}{\kappa_1} + \tilde{\rho}_i^T\rho_i), \tag{22}$$

where $\tilde{\iota}_i = \iota_i - \hat{\iota}_i$.

The derivative of (22) is presented as

$$\begin{aligned}\dot{V}_1(t) = 2\sum_{i=1}^{N} & e_{xi}^T(t)P_i(B_i\tilde{\rho}_iu_i(t) + (A_i - L_iC_i)e_{xi}(t) - L_ie_{yi}(t) \\ & + R_i(t) - \Delta_i(t)) + 2\sum_{i=1}^{N}(\Psi_i(t)\dot{\Psi}_i(t) + \frac{\tilde{\iota}_i^T\dot{\tilde{\iota}}_i}{\kappa_1} + \tilde{\rho}_i^T\dot{\tilde{\rho}}_i).\end{aligned} \tag{23}$$

From (15), one can deduce that

$$\begin{aligned}& 2{e_{xi}}^T(t)P_iB_i\tilde{\rho}_iu_i(t) + 2\tilde{\rho}_i^T\dot{\tilde{\rho}}_i \\ & = 2e_{xi}^T(t)P_iB_i\tilde{\rho}_iu_i(t) + 2\tilde{\rho}_i^T(\dot{\rho}_i - \dot{\hat{\rho}}_i) \\ & = 2e_{xi}^T(t)P_iB_i\tilde{\rho}_iu_i(t) + 2\tilde{\rho}_i^T(\dot{\rho}_i - e_{xi}^T(t)P_iB_iu_i(t)) \\ & \le 2\tilde{\rho}_i^T\dot{\rho}_i \\ & \le 2\eta_{ci},\end{aligned} \tag{24}$$

In terms of (20), one has

$$\begin{aligned}& 2{e_{xi}}^T(t)P_iR_i(t) + 2\Psi_i(t)\dot{\Psi}_i(t) + 2\frac{\tilde{\iota}_i^T\dot{\tilde{\iota}}_i}{\kappa_1} \\ & \le 2\iota_i\|e_{xi}^T(t)P_i\|\Psi_i(t) + 2\Psi_i(t)^T(\kappa_2e_{xi}(t) + \dot{e}_{xi}(t) - \dot{\xi}_i(t)) + 2\frac{\tilde{\iota}_i^T\dot{\tilde{\iota}}_i}{\kappa_1} \\ & \le 2\iota_i\|e_{xi}^T(t)P_i\|\Psi_i(t) + 2\Psi_i(t)^T(R_i(t) - \hat{R}_i(t)) + 2\frac{\tilde{\iota}_i^T\dot{\tilde{\iota}}_i}{\kappa_1} \\ & \le 2\iota_i\|e_{xi}^T(t)P_i\|\Psi_i(t) + 2\Psi_i(t)^T(\iota_i\|\Psi_i(t)\| - (\kappa_1 + \hat{\iota}_i)\Psi_i(t)) \\ & \quad - 2\tilde{\iota}_i^T(\|\Psi_i(t)\|^2 + \|e_{xi}^T(t)P_i\|\|\Psi_i(t)\|) \\ & = 2\iota_i\|e_{xi}^T(t)P_i\|\Psi_i(t) - 2\tilde{\iota}_i\|e_{xi}^T(t)P_i\|\|\Psi_i(t)\| - 2\kappa_1\|\Psi_i(t)\|^2 \\ & = -2\kappa_1\|\Psi_i(t)\|^2 + 2\hat{\iota}_i\|e_{xi}^T(t)P_i\|\|\Psi_i(t)\|.\end{aligned} \tag{25}$$

Combing (24) and (25), one can obtain

$$\begin{aligned}\dot{V}_1(t) \le & 2\sum_{i=1}^{N}e_{xi}^T(t)P_i((A_i - L_iC_i)e_{xi}(t) - L_ie_{yi}(t) - \Delta_i(t)) \\ & -2\sum_{i=1}^{N}(e_{xi}^T(t)P_iL_{ci}e_{xi}(t) - e_{xi}^T(t)P_iL_{ci}e_{xi}(t)) \\ & -2\sum_{i=1}^{N}\kappa_1\|\Psi_i(t)\|^2 + 2\sum_{i=1}^{N}\hat{\iota}_i\|e_{xi}^T(t)P_i\|\|\Psi_i(t)\| \\ & +2\sum_{i=1}^{N}\eta_{ci}\end{aligned} \tag{26}$$

Substituting (14) into (26), one has

$$\begin{aligned}\dot{V}_1(t) \leq & -2\sum_{i=1}^{N} e_{xi}^T(t)P_i\frac{P_ie_{xi}(t)}{\|e_{xi}(t)^TP_i\|^2}(\eta_{ci}-\kappa_1\|\Psi_i(t)\|^2\\ & +\hat{\iota}_i\left\|e_{xi}(t)^TP_i\right\|\Psi_i(t)-\left\|e_{xi}(t)^TP_iL_{ci}e_{xi}(t)\right\|\\ & -\left\|e_{xi}(t)^TP_iL_ie_{yi}(t)\right\|)-2\sum_{i=1}^{N} e_{xi}^T(t)P_iL_ie_{yi}(t)\\ & +2\sum_{i=1}^{N}(\eta_{ci}-\kappa_1\|\Psi_i(t)\|^2+\hat{\iota}_i\|e_{xi}^T(t)P_i\|\|\Psi_i(t)\|\\ & -e_{xi}^T(t)P_iL_{ci}e_{xi}(t))+2\sum_{i=1}^{N} e_{xi}^T(t)P_i(A_i-L_iC_i)e_{xi}(t)\\ & +2\sum_{i=1}^{N} e_{xi}^T(t)P_iL_{ci}e_{xi}(t)\\ \leq & 2\sum_{i=1}^{N} e_{xi}^T(t)P_i(A_i-L_iC_i)e_{xi}(t)+2\sum_{i=1}^{N} e_{xi}^T(t)P_iL_{ci}e_{xi}(t)\\ = & e^T((P\Gamma+PL_c)^T+(P\Gamma+PL_c))e. \end{aligned} \tag{27}$$

where $e_x=[e_{x1},e_{x2},\cdots,e_{xN}]^T$.

According to (21), one can conclude that $\dot{V}_1(t)<0$. On $\Xi_{n,2}$, similar results can be obtained. Hence, the convergence of the estimation errors is guaranteed. This completes the proof. □

Remark 4. *In this work, the estimation of the lumped disturbance is based on the assumption $R_i(t)\leq\iota_i\|\Psi_i(t)\|$, which is reasonable. The actuator fault and the external disturbance in the practical system are both bounded, and the auxiliary vector $\Psi_i(t)$ has the information of the lumped disturbance. Since the lumped disturbance is bounded, by introducing the unknown scalar ι_i, the assumption can be satisfied.*

4.3. FTCC Design

The tracking error is defined as

$$s_i=\chi_1z_i+\chi_2\sum_{j\in N_i}a_{ij}(z_i-z_j), \tag{28}$$

where $z_i=y_i(t^i_{k,n+1}h)-y_{id}(t)$, $y_{id}(t)$ is the desired reference, χ_1 and χ_2 are positive parameters.

Then, (28) can be rewritten as

$$S=[(\chi_1I_N+\chi_2\mathcal{L})\otimes I_3]Z_1, \tag{29}$$

where $S=[s_1^T,s_2^T,\cdots,s_N^T]^T$ and $Z_1=[z_1^T,z_2^T,\cdots,z_N^T]^T$. In terms of Lemma 1, one has $Z_1\to0$ as $S\to0$.

The error constraints are defined as

$$-\underline{k}_i\varepsilon_i(t)\leq s_i\leq\bar{k}_i\varepsilon_i(t), \tag{30}$$

where $\underline{k}_i$ and $\bar{k}_i$ are positive constants.

The PPF is chosen as

$$\varepsilon_i(t)=\coth(\beta_1t+\beta_2)-1+\varepsilon_{i\infty}, \tag{31}$$

where β_1 and β_2 are positive constants.

In order to facilitate controller design, (30) can be transformed as

$$s_i = \varepsilon_i(t)\Lambda(e_{is}), \tag{32}$$

where e_{is} is the transformed error, $\Lambda(e_{is}) = \frac{\bar{k}_i e^{e_{is}} - \underline{k}_i e^{-e_{is}}}{e^{e_{is}} - e^{-e_{is}}}$.

Then, one can obtain

$$e_{is} = \frac{1}{2}\ln(\frac{\underline{k}_i + \pi_i}{\bar{k}_i} - \pi_i), \tag{33}$$

where $\pi_i = s_i/\varepsilon_i$.

The derivative of (33) is presented as

$$\begin{aligned}\dot{e}_{is} &= \frac{1}{2}(\frac{1}{\pi_i + \underline{k}_i} - \frac{1}{\pi_i - \bar{k}_i})(\frac{\dot{s}_i}{\varepsilon_i} - \frac{\dot{\varepsilon}_i s_i}{\varepsilon_i^2}) \\ &= v_i(\dot{s}_i - \frac{\dot{\varepsilon}_i s_i}{\varepsilon_i}),\end{aligned} \tag{34}$$

where $v_i = \frac{1}{2\varepsilon_i}(\frac{1}{\pi_i + \underline{k}_i} - \frac{1}{\pi_i - \bar{k}_i})$.

The sliding mode manifold is designed as

$$\delta_i = \int_0^t (\varsigma_i(e_{is}^{\alpha_1} + \dot{e}_{is}^{\alpha_2}) - v_i\Omega C_i B_i\hat{\rho}_i u_i^a(t))dt + e_{is}, \tag{35}$$

where α_1 and α_2 are positive constants. ς_i is designed as

$$\varsigma_i = \frac{\alpha_a}{\alpha_b + \alpha_c \exp(-\alpha_d(\|\hat{R}_i\| + \|e_{is}\|)^{\alpha_e})},$$

where α_a, α_b, α_c, α_d, and α_e are positive constants.

The derivative of (35) is presented as

$$\begin{aligned}\dot{\delta}_i =& \varsigma_i(e_{is}^{\alpha_1} + \dot{e}_{is}^{\alpha_2}) - v_i\Omega C_i B_i\hat{\rho}_i u_i^a(t) + v_i(\dot{s}_i - \frac{\dot{\varepsilon}_i s_i}{\varepsilon_i}) \\ =& \varsigma_i(e_{is}^{\alpha_1} + \dot{e}_{is}^{\alpha_2}) - v_i\Omega C_i B_i\hat{\rho}_i u_i^a(t) + v_i\Omega C_i(A_i x_i(t) \\ &+ B_i\rho_i u_i(t) + \theta_i^{*T}\varphi_i(\hat{x}_i) + R_i(t)) - v_i\Omega\dot{y}_{id} \\ &+ v_i\chi_2\sum_{j\in N_i} l_{ij}z_j - \frac{v_i\dot{\varepsilon}_i s_i}{\varepsilon_i} \\ =& \varsigma_i(e_{is}^{\alpha_1} + \dot{e}_{is}^{\alpha_2}) + v_i\Omega C_i(A_i x_i(t) + B_i\hat{\rho}_i u_i^b(t) \\ &+ B_i\tilde{\rho}_i u_i(t) + \theta_i^{*T}\varphi_i(\hat{x}_i) + R_i(t)) \\ &- v_i\Omega\dot{y}_{id} + v_i\chi_2\sum_{j\in N_i} l_{ij}z_j - \frac{v_i\dot{\varepsilon}_i s_i}{\varepsilon_i},\end{aligned} \tag{36}$$

where $\Omega = \chi_1 + \chi_2 l_{ii}$.

Hence, the equivalent control is obtained

$$u_i^{beq}(t) = -(C_i B_i\hat{\rho}_i)^{-1}(\frac{\varsigma_i}{v_i\Omega}(e_{is}^{\alpha_1} + \dot{e}_{is}^{\alpha_2}) - \dot{y}_{id} + \Phi_{i1}(t)), \tag{37}$$

where $\Phi_{i1}(t) = C_i(A_i x_i(t) + B_i\tilde{\rho}_i u_i(t) + \theta_i^{*T}\varphi_i(\hat{x}_i) + R_i(t)) + \frac{\chi_2}{\Omega}\sum_{j\in N_i} l_{ij}z_j - \frac{\dot{\varepsilon}_i s_i}{\Omega\varepsilon_i}$.

The FTCC scheme is designed as

$$u_i^a(t) = \begin{cases} -(C_i B_i\hat{\rho}_i)^{-1}((\alpha_f + \hat{\varrho}_{1i}\varpi_1)\text{sign}(\delta_i)), t \in \Xi_{n,1}, \\ -(C_i B_i\hat{\rho}_i)^{-1}((\alpha_g + \hat{\varrho}_{2i}\varpi_2)\text{sign}(\delta_i)), t \in \Xi_{n,2}, \end{cases} \tag{38}$$

$$u_i^b(t) = -(C_iB_i\hat{\rho}_i)^{-1}(\frac{\varsigma_i}{v_i\Omega}(e_{is}^{\alpha_1} + \dot{e}_{is}^{\alpha_2}) - \dot{y}_{id} + \Phi_{i2}(t)), \tag{39}$$

where $\Phi_{i2}(t) = C_i(A_i\hat{x}_i(t) + \hat{\theta}_i^T\varphi_i(\hat{x}_i) + \hat{R}_i(t)) + \frac{\chi_2}{\Omega}\sum_{j\in N_i} l_{ij}\hat{z}_j - \frac{\dot{\varepsilon}_i\hat{s}_i}{\Omega\varepsilon_i}$, $\hat{z}_j = \hat{y}_j - y_{jd}$, $\hat{s}_i = \chi_1\hat{z}_i + \chi_2\sum_{j\in N_i} a_{ij}(\hat{z}_i - \hat{z}_j)$. α_f and α_g are positive constants, ϖ_1 and ϖ_2 are two new vectors, which will be given later, and $\hat{\varrho}_{1i}$ and $\hat{\varrho}_{2i}$ are the estimations of two unknown vectors ϱ_{1i} and ϱ_{2i}, respectively, which will also be defined later.

To save the limited communication resources, the event condition in the control channel is considered. Hence, under the ET condition of the control channel, the triggered control $u_i^b(t)$ can be rewritten as

$$u_i^{bet}(t) = \begin{cases} -(C_iB_i\hat{\rho}_i(t_c))^{-1}(\frac{\varsigma_i}{v_i\Omega}(e_{is}^{\alpha_1}(t_c) + \dot{e}_{is}^{\alpha_2}(t_c)) - \dot{y}_{id}(t_c) + \Phi_{i2}(t_c)), t \in \Xi_{n,1}, \\ -(C_iB_i\hat{\rho}_i(t_{p_{dn}+l_{dn}}))^{-1}(\frac{\varsigma_i}{v_i\Omega}(e_{is}^{\alpha_1}(t_{p_{dn}+l_{dn}}) \\ \quad + \dot{e}_{is}^{\alpha_2}(t_{p_{dn}+ldn})) - \dot{y}_{id}(t_{p_{dn}+l_{dn}}) + \Phi_{i2}(t_{p_{dn}+l_{dn}})), t \in \Xi_{n,2}, \end{cases} \tag{40}$$

where t_c is the event-triggered instant of the control channel, which is designed as

$$t_{c+1}^i = \inf\{t > t_c^i : h_i(t) > 0\}. \tag{41}$$

The triggered function is designed as

$$h_i(t) = \|e_{is}^{\alpha_1}(t) - e_{is}^{\alpha_1}(t_c)\| - e^{\mu_1} - \nu_1 \tag{42}$$

$$\text{or } \|\dot{e}_{is}^{\alpha_2}(t) - \dot{e}_{is}^{\alpha_2}(t_c)\| - e^{\mu_2} - \nu_2, \tag{43}$$

where μ_1, μ_2, ν_1, and ν_2 are positive constants.

Theorem 2. *Consider HMASs under Assumptions 1–4. The sliding mode manifold is given as (35), the triggered function is designed as (42), the control law is presented as (38) and (40), and then the sliding motion will maintain and the tracking errors of all vehicles can be guaranteed.*

Proof. Select the Lyapunov function

$$V_s(t) = \sum_{i=1}^{N}(1 - \mathcal{J})V_{s1}(t) + \mathcal{J}V_{s2}(t), \tag{44}$$

with $V_{s1}(t) = \frac{1}{2}\delta_i(t)^T\delta_i(t) + \frac{1}{2}(\varrho_{1i} - \hat{\varrho}_{1i})^2$, $\mathcal{J} = 0, t \in \Xi_{n,1}$; $V_{s2}(t) = \frac{1}{2}\delta_i(t)^T\delta_i(t) + \frac{1}{2}(\varrho_{2i} - \hat{\varrho}_{2i})^2$, $\mathcal{J} = 1, t \in \Xi_{n,2}$.

Consider that there is no DoS attack, i.e., $t \in \Xi_{n,1}$. Substituting (38) and (40) into (36), one can obtain

$$\begin{aligned} \dot{\delta}_i(t) = & \varsigma_i(e_{is}^{\alpha_1}(t) + \dot{e}_{is}^{\alpha_2}(t)) - v_i\Omega\dot{y}_{id} + v_i\Omega\Phi_{i1}(t) \\ & -\varsigma_i(e_{is}^{\alpha_1}(t_c) + \dot{e}_{is}^{\alpha_2}(t_c)) + v_i\Omega\dot{y}_{id}(t_c) - v_i\Omega\Phi_{i2}(t_c) \\ = & \varsigma_i(e_{is}^{\alpha_1}(t) - e_{is}^{\alpha_1}(t_c) + \dot{e}_{is}^{\alpha_2}(t) - \dot{e}_{is}^{\alpha_2}(t_c)) + \Phi_{i3}(t) \\ & -(\alpha_f + \hat{\varrho}_{1i}\varpi_1)\text{sign}(\delta_i), \end{aligned} \tag{45}$$

where $\Phi_{i3}(t) = -v_i\Omega\dot{y}_{id} + v_i\Omega\Phi_{i1}(t) + v_i\Omega\dot{y}_{id}(t_c) - v_i\Omega\Phi_{i2}(t_c) + (\alpha_f + \hat{\varrho}_{1i}\varpi_1)\text{sign}(\delta_i)$.

Let $\Theta_i = \|\varsigma_i(e_{is}^{\alpha_1}(t) - e_{is}^{\alpha_1}(t_c) + \dot{e}_{is}^{\alpha_2}(t) - \dot{e}_{is}^{\alpha_2}(t_c))\| + \|\Phi_{i3}(t)\|$. Then, one can obtain that Θ_i is unknown but bounded. The RBFNN is utilized to approximate the unknown part Θ_i.

$$\Theta_i = \mathcal{F}_i^T\psi_i(t) + \mathcal{M}_i. \tag{46}$$

Hence, one can obtain

$$\begin{aligned}\delta_i(t)\Theta_i &\leq \|\delta_i(t)\|\|\mathcal{F}_i^T\|\|\psi_i(t)\| + \|\delta_i(t)\|\mathcal{M}_i \\ &= \|\delta_i(t)\|\varrho_{1i}\varpi_{1i},\end{aligned} \tag{47}$$

where $\varrho_{1i} = [\|\mathcal{F}_i^T\|, \mathcal{M}_i]$, $\varpi_{1i} = [\|\psi_i(t)\|, 1]^T$. In addition, the adaptive law of ϱ_{1i} is updated as $\dot{\hat{\varrho}}_{1i} = \|\delta_i(t)\|\varpi_{1i}$.

The derivative of (44) yields that

$$\begin{aligned}\dot{V}_s(t) &\leq \sum_{i=1}^{N}(\delta_i(t)^T\dot{\delta}_i(t) + (\varrho_{1i} - \hat{\varrho}_{1i})(\dot{\varrho}_{1i} - \dot{\hat{\varrho}}_{1i})) \\ &\leq \sum_{i=1}^{N}(\|\delta_i(t)\|\varrho_{1i}\varpi_{1i} - \delta_i(t)^T(\alpha_f + \hat{\varrho}_{1i}\varpi_{1i})\text{sign}(\delta_i) \\ &\quad -(\varrho_{1i} - \hat{\varrho}_{1i})\|\delta_i(t)\|\varpi_{1i}) \\ &= \sum_{i=1}^{N}(\|\delta_i(t)\|(\varrho_{1i}\varpi_{1i} - \alpha_f - \hat{\varrho}_{1i}\varpi_{1i}) \\ &\quad -(\varrho_{1i} - \hat{\varrho}_{1i})\|\delta_i(t)\|\varpi_{1i}) \\ &\leq -\sum_{i=1}^{N}\alpha_f\|\delta_i(t)\|.\end{aligned} \tag{48}$$

Consider that the DoS attack is launched, i.e., $t \in \Xi_{n,2}$. Similar results can be obtained through similar derivations. Hence, it can be concluded that $\dot{V}_s(t) \leq 0$, which implies that the sliding motion will maintain and the convergence of e_{is} is guaranteed. In terms of the property of the PPF, the boundedness of e_{is} implies that the tracking errors s_i are also bounded within the predefined bounds specified by (30). This ends the proof. □

Remark 5. *It can be easily seen from (10) that the minimum time interval will be no less than h, which implies that the time interval between two adjacent data release times will not be less than the sampling period. Hence, the Zeno behavior can be avoided in the sensor channel. A similar analysis can be applied in the controller channel. Therefore, the Zeno behavior can be also avoided in the controller channel.*

Remark 6. *In some existing literature [37,38], the control input is directly set to zero. It does not consider how to utilize an observer to guarantee the safe and stable operation of the system. The existing results about event-triggered mechanism concentrates on either the sensor channel or the control channel. It is challenging to take both sensor and control channels into account, simultaneously. Hence, the novelty of this work is that an observer-based ET-FTCC scheme is proposed via dual-terminal triggered mechanisms with prescribed performance.*

5. Simulation Studies

In this section, the efficiency of the presented ET-FTCC scheme is verified with actuator faults and external disturbances under DoS attacks.

5.1. Simulation Conditions

The HMASs containing two UAVs and two UGVs are considered. The topology of the HMASs is described in Figure 5.

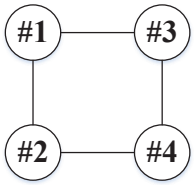

Figure 5. Communication topology graph.

The system parameters are given as $m_{ai} = 2$ kg, $d_{ix} = d_{iy} = d_{iz} = 0.012\ \mathrm{N \cdot s \cdot rad^{-1}}$, $M_{gi} = 10$ kg, $J_{gi} = 1\ \mathrm{N \cdot s \cdot rad^{-1}}$, $L_{gi} = 0.5$ m. The initial values are $x_{11}(0) = [-0.9, 2, 2.5]^T$, $x_{21}(0) = [-0.4, -1, 0.5]^T$, $x_{31}(0) = [2.2, -2.5, 0]^T$, $x_{41}(0) = [-1.5, 1.5, 0]^T$, $x_{12}(0) = [0.1, 0.2, 0.5]^T$, $x_{22}(0) = [0.3, 0.6, 0.4]^T$, $x_{32}(0) = [0.1, 0.3, 0]^T$, and $x_{42}(0) = [0.2, 0.4, 0]^T$. The parameters are selected as $\alpha_1 = 0.7$, $\alpha_2 = 1.2$, $\alpha_a = 0.9$, $\alpha_b = 1.3$, $\alpha_c = 1$, $\alpha_f = 0.2$, $\alpha_g = 0.5$, $\mu_1 = 0.4$, $\mu_2 = 0.4$, $\nu_1 = 0.01$, and $\nu_2 = 0.01$. The prescribed performance function parameters are given as $\beta_1 = 0.3$, $\beta_2 = 0.3$, $\varepsilon_{i\infty} = 3$. The external disturbances are given as $d_1 = [0.3\sin(t), 0.4, 0.2\cos(t)]^T$, $d_2 = [0.25, 0.3\sin(t), 0.2]^T$, $d_3 = [0.3\sin(t), 0.2, 0]^T$, and $d_4 = [0.5\cos(t), 0.1, 0]^T$. The actuator faults are encountered by the followers UAV#1 and UGV#4, and they are given as $\rho_{11} = I_3$, $u_{11b} = [0, 0, 0]^T$ for $t < 9$ s, and $\rho_{11} = \mathrm{diag}\{0.9, 1, 0.8\}$, $u_{11b} = [0.2, 0.3, 0.15]^T$ for $t \geq 9$ s, $\rho_{41} = \mathrm{diag}\{1, 1, 0\}$, $u_{41b} = [0, 0, 0]^T$ for $t < 15$ s, and $\rho_{41} = \mathrm{diag}\{0.8, 0.9, 0\}$, $u_{41b} = [0.3, 0.2, 0]^T$ for $t \geq 15$ s.

The performance of the presented ET-FTCC scheme is compared with the control scheme in [39]. To further quantitatively evaluate the control performance, the X-direction, Y-direction, and Z-direction tracking error metric (TEM) are defined as

$$\mathrm{XTEM} = \sqrt{\frac{1}{4}\sum_{i=1}^{4}|s_{ix}|^2}, \mathrm{YTEM} = \sqrt{\frac{1}{4}\sum_{i=1}^{4}|s_{iy}|^2}, \mathrm{ZTEM} = \sqrt{\frac{1}{2}\sum_{i=1}^{2}|s_{iz}|^2}.$$

5.2. Simulation Results

The simulation results are presented in Figures 6–8. The tracking errors of UAVs and UGVs in the X-direction, Y-direction, and Z-direction are depicted in Figure 6. It can be observed from Figure 6 that the tracking errors achieve good performance, which are confined within the prescribed error bounds $(\underline{k}_i\varepsilon_i, \bar{k}_i\varepsilon_i)$. In addition, the active period of the DoS attack is denoted by the green shadow, while the rest parts denote that there is no DoS attack. To further show the advantages of the proposed scheme, a simulation comparison of the control approach in [39] is also carried out.

From Figure 6, one can determine that the tracking performance will degraded when the DoS attacks are active. It can be observed that the proposed scheme in this work has better recovery performance under DoS attacks. The tracking performance can recover soon when the attackers are sleeping. Meanwhile, the approach in [39] cannot ensure good performance when the DoS attacks are active. As depicted in Figure 7, the proposed scheme has better recovering abilities than the approach in [39], which means that the tracking performance is recovered by utilizing the presented scheme, even subjected to actuator faults and external disturbances under DoS attacks. Figure 8 shows the release times and intervals of the event-triggered mechanism. It can be observed from Figure 8 that the communication burden is reduced Hence, the efficiency of the presented decentralized adaptive ET-FTCC scheme with prescribed performance in the presence of actuator faults, external disturbances, and DoS attacks is verified.

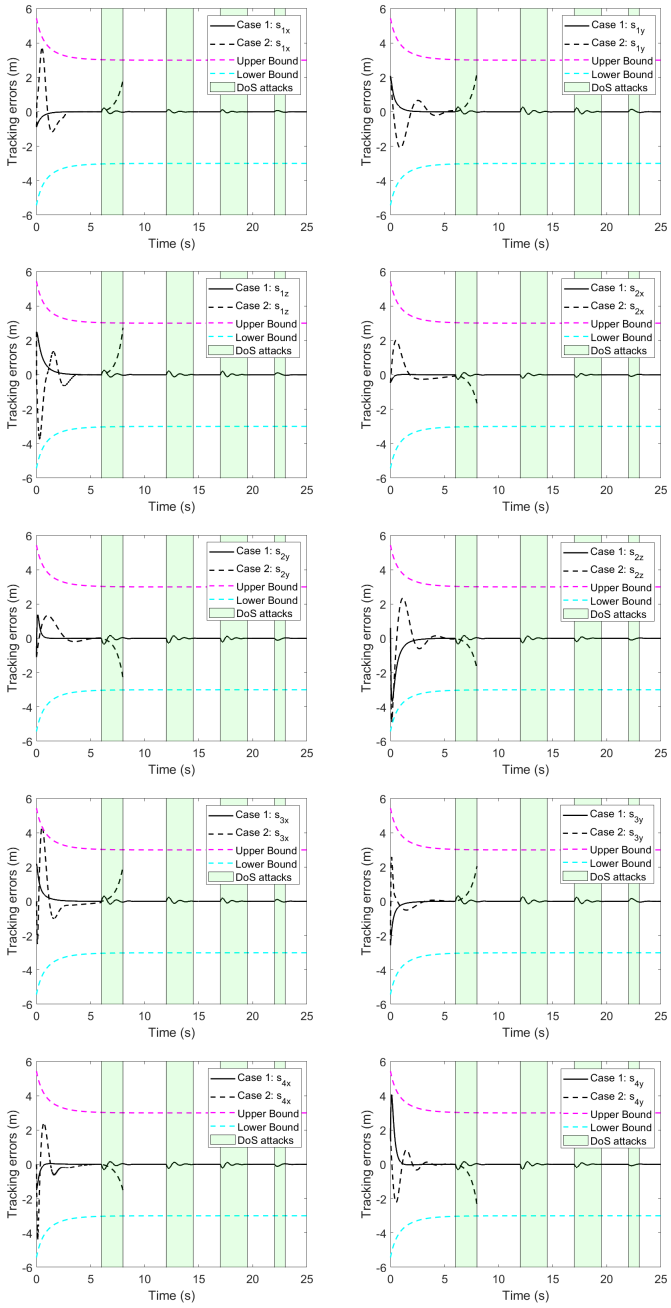

Figure 6. Position errors of UAVs and UGVs. (Case 1: presented method; case 2: method in [39]).

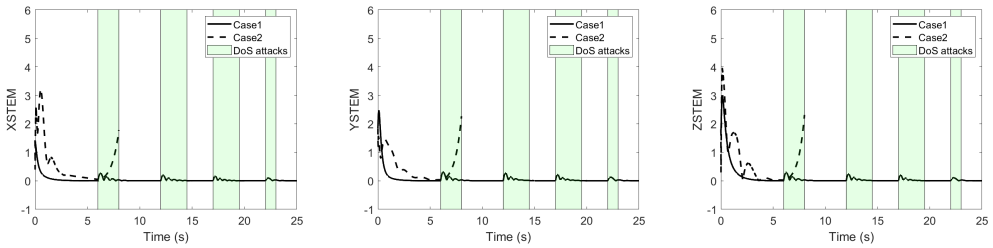

Figure 7. XTEM, YTEM, and ZTEM. (Case 1: presented method; case 2: method in [39]).

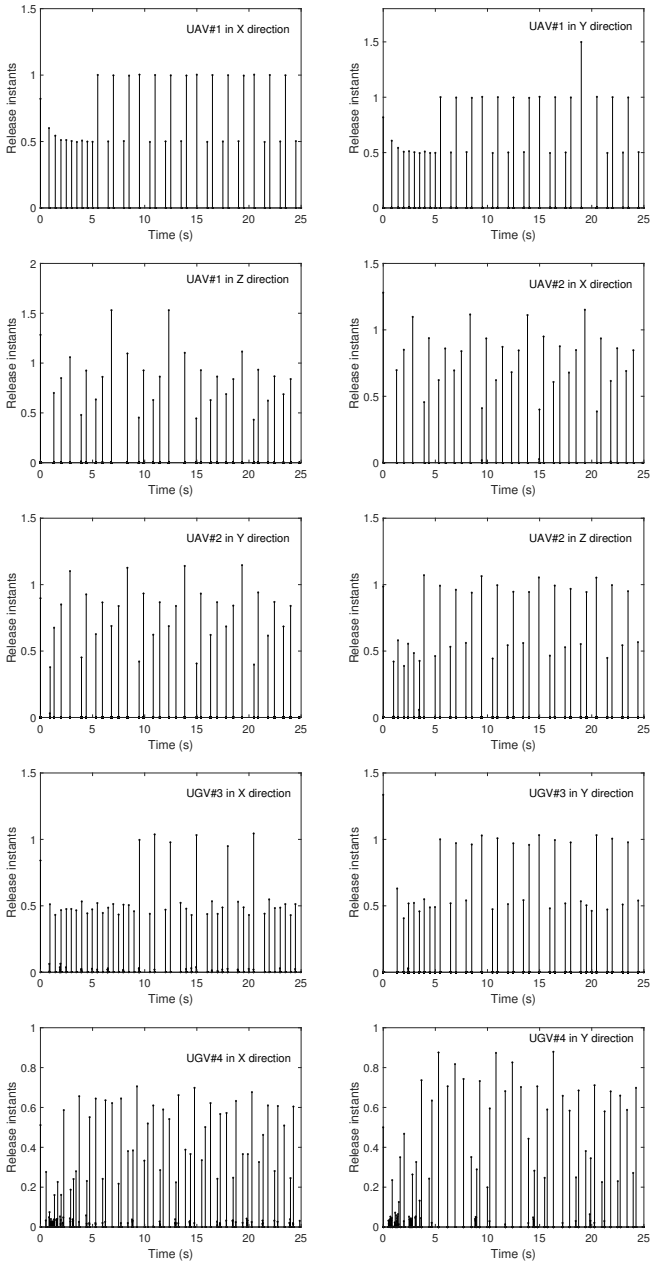

Figure 8. Release instants and intervals of UAVs and UGVs.

6. Conclusions

In this paper, the ET-FTCC is investigated for HMASs with actuator faults and external disturbances under DoS attacks. The composite observer is designed to obtain the information of state and lumped disturbance, which is used to design the controller. After that, the event-triggered sliding mode FTCC scheme is presented to compensate for actuator faults and external disturbances and defend against DoS attacks. The tracking errors are bounded within the prescribed boundary. The effectiveness of the proposed method is verified by qualitative analysis and quantitative analysis of the simulation results. This study can enhance the security and reliability of heterogeneous multi-agent systems, providing technical support for the safe operation of unmanned systems.

This article mainly solves the FTCC problem of second-order nonlinear heterogeneous multiagent systems, and further research is needed for the FTCC problem of higher-order nonlinear heterogeneous multi-agent systems. In addition, the DoS attacks are considered in this paper. However, the heterogeneous multiagent systems may encounter multiple

cyber attacks, such as DoS attacks and deception attacks. In order to solve the multiple cyber attacks, a multiple cyber attack model should be modeled first. Combining the characteristics of the attack model and the unified model of the heterogeneous multiagent systems, the FTCC scheme will be investigated to compensate the influence of the faults under multiple cyber attacks, which is one of our future works.

Author Contributions: Conceptualization, S.L.; methodology, S.L.; software, S.L.; validation, S.L.; writing—original draft preparation, S.L.; writing—review and editing, S.L. and J.H.; supervision, J.H.; project administration, J.H.; funding acquisition, J.H. All authors have read and agreed to the published version of the manuscript.

Funding: This research was funded by the Natural Science Foundation of China (No. 92367109), Aeronautical Science Foundation of China (No. 2023000144001).

Data Availability Statement: No new data were created or analyzed in this study.

Conflicts of Interest: The authors declare no conflicts of interest.

References

1. Liu, C.; Jiang, B.; Wang, X.; Yang, H.; Xie, S. Distributed Fault-Tolerant Consensus Tracking of Multi-Agent Systems under Cyber-Attacks. *IEEE/CAA J. Autom. Sin.* **2022**, *9*, 1037–1048. [CrossRef]
2. Zuo, Z.; Cao, X.; Wang, Y.; Zhang, W. Resilient Consensus of Multiagent Systems Against Denial-of-Service Attacks. *IEEE Trans. Syst. Man Cybern. Syst.* **2022**, *52*, 2664–2675. [CrossRef]
3. Shen, Q.; Jiang, B.; Shi, P. Adaptive Fault Diagnosis for T–S Fuzzy Systems with Sensor Faults and System Performance Analysis. *IEEE Trans. Fuzzy Syst.* **2014**, *22*, 274–285. [CrossRef]
4. Wu, J.; Cui, P. Cooperative Adaptive Fuzzy Control for the Synchronization of Nonlinear Multi-Agent Systems under Input Saturation. *Mathematics* **2024**, *12*, 1426. [CrossRef]
5. Guo, X.; Wang, C.; Dong, Z.; Ding, Z. Adaptive Containment Control for Heterogeneous MIMO Nonlinear Multiagent Systems With Unknown Direction Actuator Faults. *IEEE Trans. Autom. Control* **2023**, *68*, 5783–5790. [CrossRef]
6. Liu, Y.; Su, H. Second-Order Consensus for Multiagent Systems with Switched Dynamics and Sampled Position Data. *IEEE Trans. Syst. Man Cybern. Syst.* **2022**, *52*, 4129–4137. [CrossRef]
7. Jiang, B.; Shen, Q.; Shi, P. Neural-networked adaptive tracking control for switched nonlinear pure-feedback systems under arbitrary switching. *Automatica* **2015**, *61*, 119–125. [CrossRef]
8. Jiang, B.; Zhang, K.; Shi, P. Integrated Fault Estimation and Accommodation Design for Discrete-Time Takagi-Sugeno Fuzzy Systems With Actuator Faults. *IEEE Trans. Fuzzy Syst.* **2011**, *19*, 291–304. [CrossRef]
9. Chen, K.; Gu, Y.; Lin, H.; Zhang, Z.; Zhou, X.; Wang, X. Guaranteed Performance Event-Triggered Adaptive Consensus Control for Multiagent Systems under Time-Varying Actuator Faults. *Mathematics* **2024**, *12*, 1528. [CrossRef]
10. Wu, Y.; Li, J.; Liu, L.; Wu, C. Distributed adaptive practical formation tracking for multi-agent systems with actuator faults. *Int. J. Robust Nonlinear Control* **2023**, *33*, 1633–1654. [CrossRef]
11. Wang, Z.; Wu, Y.; Liu, L.; Zhang, H. Adaptive Fault-Tolerant Consensus Protocols for Multiagent Systems with Directed Graphs. *IEEE Trans. Cybern.* **2020**, *50*, 25–35. [CrossRef] [PubMed]
12. Xiao, S.; Dong, J. Distributed Adaptive Fuzzy Fault-Tolerant Containment Control for Heterogeneous Nonlinear Multiagent Systems. *IEEE Trans. Syst. Man Cybern. Syst.* **2022**, *52*, 954–965. [CrossRef]
13. Wang, J.; Gui, Z.; Sun, J.; Xie, X.; Meng, Q. Distributed Fault-Tolerant Control of Nonlinear Multiagent Systems With Generally Uncertain Semi-Markovian Switching Topologies. *IEEE Trans. Autom. Sci. Eng.* **2024**. [CrossRef]
14. Zhao, L.; Zhao, F.; Che, W.W. Distributed adaptive fuzzy fault-tolerant control for multi-agent systems with node faults and denial-of-service attacks. *Inf. Sci.* **2023**, *631*, 385–395. [CrossRef]
15. Deng, C.; Wen, C. Distributed Resilient Observer-Based Fault-Tolerant Control for Heterogeneous Multiagent Systems Under Actuator Faults and DoS Attacks. *IEEE Trans. Control Netw. Syst.* **2020**, *7*, 1308–1318. [CrossRef]
16. Zhang, D.; Liu, L.; Feng, G. Consensus of Heterogeneous Linear Multiagent Systems Subject to Aperiodic Sampled-Data and DoS Attack. *IEEE Trans. Cybern.* **2019**, *49*, 1501–1511. [CrossRef]
17. Wan, Y.; Wen, G.; Yu, X.; Huang, T. Distributed Consensus Tracking of Networked Agent Systems Under Denial-of-Service Attacks. *IEEE Trans. Syst. Man Cybern. Syst.* **2021**, *51*, 6183–6196. [CrossRef]
18. Pan, K.; Lyu, Y.; Pan, Q. Adaptive Formation for Multiagent Systems Subject to Denial-of-Service Attacks. *IEEE Trans. Circuits Syst. I* **2022**, *69*, 3391–3401. [CrossRef]
19. Lu, L.T.; Zhu, S.L.; Wang, D.M.; Han, Y.Q. Distributed adaptive fault-tolerant control with prescribed performance for nonlinear multiagent systems. *Commun. Nonlinear Sci.* **2024**, *138*, 108222. [CrossRef]
20. Gao, Z.; Zhang, Y.; Guo, G. Finite-Time Fault-Tolerant Prescribed Performance Control of Connected Vehicles with Actuator Saturation. *IEEE Trans. Veh. Technol.* **2023**, *72*, 1438–1448. [CrossRef]

21. Zhang, L.; Che, W.W.; Chen, B.; Lin, C. Adaptive Fuzzy Output-Feedback Consensus Tracking Control of Nonlinear Multiagent Systems in Prescribed Performance. *IEEE Trans. Cybern.* **2023**, *53*, 1932–1943. [CrossRef] [PubMed]
22. Ding, Z.; Wang, H.; Sun, Y.; Qin, H. Adaptive prescribed performance second-order sliding mode tracking control of autonomous underwater vehicle using neural network-based disturbance observer. *Ocean Eng.* **2022**, *260*, 111939. [CrossRef]
23. Gong, J.; Jiang, B.; Ma, Y.; Mao, Z. Distributed Adaptive Fault-Tolerant Formation-Containment Control with Prescribed Performance for Heterogeneous Multiagent Systems. *IEEE Trans. Cybern.* **2023**, *53*, 7787–7799. [CrossRef] [PubMed]
24. Mousavian, M.; Atrianfar, H. Resilient Event-triggered Containment Control of Multi-Agent Systems under Asynchronous DoS Attacks and Disturbances. *IEEE Trans. Control Netw. Syst.* **2024**. [CrossRef]
25. Cheng, Z.; Yue, D.; Hu, S.; Ge, H.; Chen, L. Distributed event-triggered consensus of multi-agent systems under periodic DoS jamming attacks. *Neurocomputing* **2020**, *400*, 458–466. [CrossRef]
26. Tang, Y.; Zhang, D.; Shi, P.; Zhang, W.; Qian, F. Event-Based Formation Control for Nonlinear Multiagent Systems Under DoS Attacks. *IEEE Trans. Autom. Control* **2021**, *66*, 452–459. [CrossRef]
27. Ye, D.; Yang, X. Distributed event-triggered consensus for nonlinear multi-agent systems subject to cyber attacks. *Inf. Sci.* **2019**, *473*, 178–189. [CrossRef]
28. Liu, Y.; Jia, Y. Event-triggered consensus control for uncertain multi-agent systems with external disturbance. *Int. J. Syst. Sci.* **2019**, *50*, 130–140. [CrossRef]
29. Li, J.; Yang, Z.; Mu, X.; Wu, X. Passivity-based Event-triggered Fault Tolerant Control for Nonlinear Networked Control System with Actuator Failures and DoS Jamming Attacks. *J. Franklin Inst.* **2020**, *357*, 9288–9307. [CrossRef]
30. Sun, L.; Zheng, Z. Disturbance Observer-Based Robust Saturated Control for Spacecraft Proximity Maneuvers. *IEEE Trans. Control Syst. Technol.* **2018**, *26*, 684–692. [CrossRef]
31. He, W.; Sun, Y.; Yan, Z.; Yang, C.; Li, Z.; Kaynak, O. Disturbance Observer-Based Neural Network Control of Cooperative Multiple Manipulators With Input Saturation. *IEEE Trans. Neural Netw. Learn. Syst.* **2020**, *31*, 1735–1746. [CrossRef] [PubMed]
32. Ma, X.; Yang, L.; Ma, L.; Dong, W.; Jin, M.; Zhang, L.; Yang, F.; Lin, Y. Consensus tracking control for uncertain non-strict feedback multi-agent system under cyber attack via resilient neuroadaptive approach. *Int. J. Robust Nonlinear Control* **2022**, *32*, 4251–4280. [CrossRef]
33. Xiang, X.; Liu, C.; Su, H.; Zhang, Q. On decentralized adaptive full-order sliding mode control of multiple UAVs. *ISA Trans.* **2017**, *71*, 196–205. [CrossRef]
34. Du, H.; Zhu, W.; Wen, G.; Duan, Z.; Lü, J. Distributed Formation Control of Multiple Quadrotor Aircraft Based on Nonsmooth Consensus Algorithms. *IEEE Trans. Cybern.* **2019**, *49*, 342–353. [CrossRef] [PubMed]
35. Dong, X.; Hua, Y.; Zhou, Y.; Ren, Z.; Zhong, Y. Theory and Experiment on Formation-Containment Control of Multiple Multirotor Unmanned Aerial Vehicle Systems. *IEEE Trans. Autom. Sci. Eng.* **2019**, *16*, 229–240. [CrossRef]
36. Aghaeeyan, A.; Abdollahi, F.; Talebi, H. UAV-UGVs cooperation: With a moving center based trajectory. *Rob. Auton. Syst.* **2015**, *63*, 1–9. [CrossRef]
37. Lu, A.Y.; Yang, G.H. Input-to-State Stabilizing Control for Cyber-Physical Systems with Multiple Transmission Channels Under Denial of Service. *IEEE Trans. Autom. Control* **2018**, *63*, 1813–1820. [CrossRef]
38. Xu, W.; Hu, G.; Ho, D.W.C.; Feng, Z. Distributed Secure Cooperative Control Under Denial-of-Service Attacks from Multiple Adversaries. *IEEE Trans. Cybern.* **2020**, *50*, 3458–3467. [CrossRef]
39. Qin, J.; Ma, Q.; Gao, H.; Zheng, W.X. Fault-Tolerant Cooperative Tracking Control via Integral Sliding Mode Control Technique. *IEEE/ASME Trans. Mechatronics* **2018**, *23*, 342–351. [CrossRef]